THE ASTROPHYSICAL JOURNAL, 494:605–613, 1998 February 20

THREE-DIMENSIONAL NON-LTE RADIATIVE TRANSFER OF CS IN CLUMPY DENSE CORES

Y.-S. PARK
Korea Astronomy Observatory, San 36-1, Hwaam-dong, Yusung, Taejon, 305-348, Korea
AND
S. S. HONG
Department of Astronomy, Seoul National University, Seoul, 151-742, Korea
Received 1997 April 29; accepted 1997 September 29

ABSTRACT

With a Monte Carlo radiative transfer code we have investigated excitation conditions of the CS molecule in dense cores and synthesized line profiles for several transitions of both CS and $C^{34}S$. We took two kinds of models of the dense core: a clumpy and a smooth model. In the clumpy model, the core is composed of many small clumps, whose volume filling factor f is unity in the central region of $r \leq 0.2R$ and then declines as $f \propto r^{-1.5}$. However, H_2 number density in the clump is kept constant and also independent of the clump position. The mean number density, $n_{H_2}(r)$, is thus constant in the central part and then decreases as the same power law. In the smooth model, the gas fills the core completely, and its *local* density exactly follows the mean density of the clumpy model. For both models, each clump has thermal as well as bulk motions, velocity dispersion of the latter being proportional to $r^{0.5}$.

In the clumpy structured core, the excitation temperature of the CS transitions is found to be generally constant over an entire region. As a consequence, the synthesized profile is of a Gaussian shape superposed with some wiggles, which reflects the existence of clumps under the bulk motion. The trend of flat distribution of excitation temperature becomes more prominent for optically thin transitions of the rarer species $C^{34}S$. The profiles develop flat-top features with minor wiggles only when the core becomes extremely thick in the optical sense. On the other hand, wider profiles that have self-absorption are synthesized in the smooth core. The self-absorption is formed by a steep gradient in the radial distribution of the excitation temperature. For optically thin $C^{34}S$ transitions, both the clumpy and the smooth cores exhibit profiles close to a Gaussian shape.

Comparing line parameters derived in the Monte Carlo code and those by the large-scale velocity gradient calculations, we found that only the clumpy models can give correct estimations of the density and abundance of the cores. Moreover, we have shown that clump parameters, such as clump size and number of clumps in a beam, are reasonably estimated by Tauber's simple method.

Since the opaque line reflects properties of a region of $\tau \sim 1$, local unbalance of bulk velocity distribution in the core, for instance, often results in a blue peak stronger than the red peak in the CS line profiles. Thus it should be noted that a combination of this feature of the optically thick line and the single peak of the thin one may not necessarily imply a signature of infall.

Subject headings: ISM: clouds — ISM: molecules — molecular processes — radiative transfer

1. INTRODUCTION

Cold dense cores have been known to be the sites of low-mass star formation. From the extensive studies of Myers's group (Myers et al. 1983; Myers & Benson 1983; Goodman et al. 1993; Caselli & Myers 1995), their association with young stars and basic physical quantities, such as density, size, and temperature, are understood. Along with those observational progresses, Shu and his colleagues have provided firm theoretical grounds on the formation of low-mass stars (Shu 1977; Shu et al. 1987; Shu 1991). Recently it was claimed that spectroscopic evidence of infall motion to form protostars was observed in these cores (Zhou et al. 1993; Zhou et al. 1994a; Zhou 1995; Myers et al. 1995; Zhou et al. 1996).

For observational studies of dense cores, molecular transitions of CO, NH_3, and CS have been widely used. One of the features suspected from the observations is the clumpiness of cores. According to Snell et al. (1984), there was little change in the volume density, but an order of magnitude variation of the CS column density across a core. It can be understood if we assume that the dense core is composed of many small clumps. The fact that a virial mass estimated by line width is less than a mass estimated by density and size is often quoted as evidence of the clumped dense core (Zhou et al. 1989). Although there are also arguments against the above statement (Fuller 1989 and references therein), we may say that the dense cores are clumpy to some extent. This idea may also be supported by a recent interferometric observation, by Zhou, Evans, & Wang (1996), and by the analogy of the generally accepted notion that molecular *clouds* have a clumpy structure (Tauber 1996 and references therein).

In order to understand the characteristics of the clumpy cores, it is crucial to investigate how line emissions are related to the physical properties of clumps, and how they are compared with those formed in a smoothly varying core. However, it involves severe complexity, since three-dimensional modeling is unavoidable. By this reason, there have been a few standard treatments of the CS radiative transfer (Liszt & Leung 1977; Walker et al. 1994), but little work on the radiative transfer in the clumpy system. Martin, Sanders, & Hills (1984), Kwan & Sanders (1986), and Tauber (1996) dealt with the problem, but excitation condition was usually assumed to be in the LTE or large-

scale velocity gradient (LVG) conditions. Park & Hong (1995) and Park, Hong, & Minh (1996) recently developed a three-dimensional radiative transfer code that incorporates statistical equilibrium conditions in the molecular clouds. Juvela (1997) has elaborated a similar code, focusing mainly on warmer cores in massive star-forming regions. The goal of this work is to explore the formation mechanism of the CS lines that trace the dense region in the complex system by applying our code to *cold* dense cores for the CS rotational transitions. It will help us to understand the features of observed lines in the context of self-absorption and to unveil the properties of clumps.

In § 2 the models of dense cores are described. Here we will consider two kinds of models: the clumpy (CL) core model and the smoothly (SM) varying core model. In § 3 we examine excitation conditions and resulting line profiles for the two kinds of models. In § 4 we discuss the accuracy of the LVG and LTE approximation, the derivation of clump parameters, and the possible pitfall in interpreting asymmetric self-absorption of an optically thick line. Finally, a summary and conclusion are given in § 5.

2. TWO KINDS OF DENSE CORE MODELS

We choose the CS molecule as a probe of the clumpy core because it has many transitions in the millimeter-wave range, enabling multitransitional studies. Since the energy-level structure of CS is simple, the treatment of radiative transfer is easier than that for other molecules tracing density. Moreover, CS is considered to be chemically stable (Zhou et al. 1993). Typical CS abundance, relative to molecular hydrogen, $X(\mathrm{CS}) = 4 \times 10^{-9}$, was obtained from Zhou et al. (1993), and the isotope abundance ratio $X(\mathrm{CS})/X(\mathrm{C}^{34}\mathrm{S})$ was fixed to 20. We consider 11 lowest energy levels, and collisional cross sections are taken from Green & Chapman (1978).

The radiative transfer code used in this paper is based on the three-dimensional Monte Carlo algorithm developed by Park & Hong (1995). The Monte Carlo scheme simulates what really happens as photons propagate inside the system. Initially the photons come from the 2.7 K background radiation and are generated spontaneously inside the core. The direction of photon propagation is isotropic, and the frequency distribution is flat for the background radiation, whereas it is Gaussian for the spontaneous emission. As photons go through the core, they are absorbed by molecules and result in stimulated emission.

Since we cannot follow all the photons, we replace them by a certain number of *model* photons, which is usually $\sim 10^6$ in this calculation. The model photons are followed until they finally escape the core or are attenuated to a negligible level. While tracing all the model photons in this way, we accumulate, for each cell, the number of de-excitations by all the model photons, which is just the de-excitation rate of the cell. With the de-excitation rate, statistical equilibrium equation is then solved.

In order to count the number of photons causing the spontaneous emissions, we should know populations of the molecules at every energy level. Thus the starting point of the Monte Carlo simulation is to assume the level populations for the cells. Then the model photons are traced and the number of de-excitations is obtained. The statistical equilibrium equation is then solved to yield a new set of level populations. This process continues until the level population converges. Finally, excitation conditions of the system are readily known, and line profiles are calculated from an integration of the source function along a line of sight.

The dense core is modeled as follows: cubic cells stacked side by side, whose number is $\sim(4\pi/3)15^3$, are taken from $31 \times 31 \times 31$ rectangular grids to form a rugged sphere as a whole. By assigning nonzero density to some of the cells, clumpy structure is realized. With an adjustment of the distribution of clumps, i.e., the nonzero density cells, we can control the geometry of the model core. In the former study on the general molecular clouds (Park & Hong 1995; Park et al. 1996), we uniformly distributed the clumps over the sphere. However in the case of a dense core, we cannot expect such a situation. Based on Snell et al. (1984), we allow the clumps to be more densely distributed in the central part than in the outer part. From these speculations, the volume filling factor of the clumps, f, can be expressed as $f \propto r^{-\alpha}$. Considering that there should be a flattening of density in the central part of the core, we finally determine the distribution of the clumps as

$$f(r) = \begin{cases} 1 & \text{for } 0 \le r \le 0.2R\ , \\ (r/0.2R)^{-1.5} & \text{for } 0.2R \le r \le R\ . \end{cases} \tag{1}$$

As for the clump density, its radial dependence is not well known. Since we want to make the model as simple as possible, the clump density $n^0_{\mathrm{H}_2}$ is assumed to be independent of the clump's position and also constant within a clump. Then the radial dependence of the *average* density $n_{\mathrm{H}_2}(r)$ is the same as the above expression, i.e.,

$$n_{\mathrm{H}_2}(r) = \begin{cases} n^0_{\mathrm{H}_2} & \text{for } 0 \le r \le 0.2R\ , \\ n^0_{\mathrm{H}_2}(r/0.2R)^{-1.5} & \text{for } 0.2R \le r \le R\ . \end{cases} \tag{2}$$

The power index, -1.5, is based on the TNT model (Fuller & Myers 1992). Actually the density distribution of the TNT model is of the form $\propto(r^{-1} + r^{-2})$, but is approximated as in the above equation for simplicity.

As we can see from equation (2), f drops to 0.09 at the surface of the core. An averaged volume filling factor over the whole sphere is $\bar{f} = 0.17$, and that over a cylinder-like volume associated with line emission is 0.40 (see § 3.2). We will carry out calculations for the density of the clump varying from 1×10^4 to 3×10^5 cm^{-3}. For simplicity we neglected interclump matter.

We adopt the core size $R = 0.3$ pc from Zhou et al. (1989) and the uniform kinetic temperature $T_k = 10$ K. For the velocity field, we consider two types of motions. One is the thermal motion inside the clump, which is characterized by a velocity dispersion σ_{thr}. We may be able to add microturbulence, but assume that it is determined solely by the kinetic temperature of the clump so that $\sigma_{\mathrm{thr}} = 0.062$ km s^{-1} for the CS. The other is the bulk motion of the clumps, σ_{blk}. It can either be microturbulent or macroturbulent, depending on the optical depth of the transition. Following Fuller & Myers (1992), we assume that $\sigma_{\mathrm{blk}}(r) = 0.5(r/R)^{1/2}$ km s^{-1}. Thus the bulk motion is much larger than the thermal motion over most of the region of the core and dominates the width of synthesized line profile. As we have just quoted the functional form of $n_{\mathrm{H}_2}(r)$ and $\sigma_{\mathrm{blk}}(r)$ from the TNT model, the model is far from consistent in the dynamical point of view (Walker et al. 1994). We simply try to model the core as realistically as possible in a reasonable range of parameters.

We will call the above-mentioned model the "CL model." For comparison, we consider the SM model, where all the cells are filled with matter ($f = 1$), and the density of the cell varies smoothly with the same form as in equation (2). In this model, $n^0_{H_2}$ is simply a scaling density. By keeping R unchanged, we make the total mass the same for both models. We also use the same kinetic temperature and velocity field for the SM model as in the CL model. In the SM model, the *clump* lose its meaning; all the *cells* that compose the core undergo the bulk motion with a given velocity distribution. One may think the SM model is a simple variant of the model by Liszt & Leung (1977); however, the two models differ from each other in the nature of turbulence. The SM model takes into account the bulk motion, while the model of Liszt & Leung (1977) only incorporates microturbulent motion, which is one of the advantages of three-dimensional radiative transfer.

3. RESULTS

3.1. *Excitation Status*

Figure 1 shows the distribution of T_{ex} of CS as a function of radial distance for both kinds of models. Since T_{ex} will only have radial dependence, the volume of the core is divided into 15 concentric shells, whose radial distances are equally spaced. Then the values of T_{ex} s in each shell are averaged and displayed in the figure. Because there is a small number of cells in the very central part of the core, T_{ex} in that region is not shown. In the figure, $\pm 1\ \sigma$ levels of noise are shown as error bars. Fluctuations are actually dependent upon the radial distance; thus, values near $r/R = 0.5$ are displayed. Generally the noise in the outer part of the core is smaller than these.

The figure shows the gradual decrease of the T_{ex} along the radial distance in the SM model as expected. If $n^0_{H_2} \gtrsim 3 \times 10^5\ \mathrm{cm}^{-3}$, even the $J = 5$–4 transition becomes thermalized in the central part. The $J = 1$–0 transition is thermalized near the center for the $n^0_{H_2} \gtrsim 3 \times 10^4\ \mathrm{cm}^{-3}$. For the $n^0_{H_2} \lesssim 1 \times 10^4\ \mathrm{cm}^{-3}$, the collisional process plays little role for most of the transitions in the whole region of the core, so that $T_{ex} \simeq 2.7$ K.

The excitation condition of the CL model is quite different from that of the SM model, although the average density distribution is the same. The most distinctive feature of the CL model is that T_{ex} is generally higher, and its distribution is flatter than that of the SM model. The reason for the uniformity of T_{ex} can be found from the fact that, due to clumpiness, the background radiation can easily penetrate the core, and radiation from the clumps can propagate with less attenuation. Thus the radiation field inside the core is not so dependent upon the location, resulting in a nearly uniform distribution of T_{ex}.

Figure 2 shows the excitation status of the $C^{34}S$. Suprathermal excitation is noted in the $J = 1$–0 transition at high density, $n^0_{H_2} \gtrsim 3 \times 10^5\ \mathrm{cm}^{-3}$. In the figure, the tendency toward the flat excitation condition is more obvious in the CL model. For lower density and for higher transition, the trend is even stronger. Another point to note is the exact coincidence of T_{ex} in the range $r/R < 0.2$ for *all* pairs between the CL and the SM groups. Since the central region has the same structure for both CL and SM models, the result implies that the excitation status of the central region is determined solely by the central part and the background radiation. The outer part plays no role in determining T_{ex} at the central part. That will be characteristic of an optically thin system. The degree of coincidence of T_{ex}, at the same time, proves the accuracy of the Monte Carlo calculations.

From Figures 1–2, we cannot expect the similarity of T_{ex} between isotopes, which is usually assumed in the case of CO-^{13}CO pairs. It is even true for lower transitions at higher density.

3.2. *Line Profiles*

Synthesized profiles of the CS transitions for both models are shown in Figure 3. To reduce statistical fluctuations, we

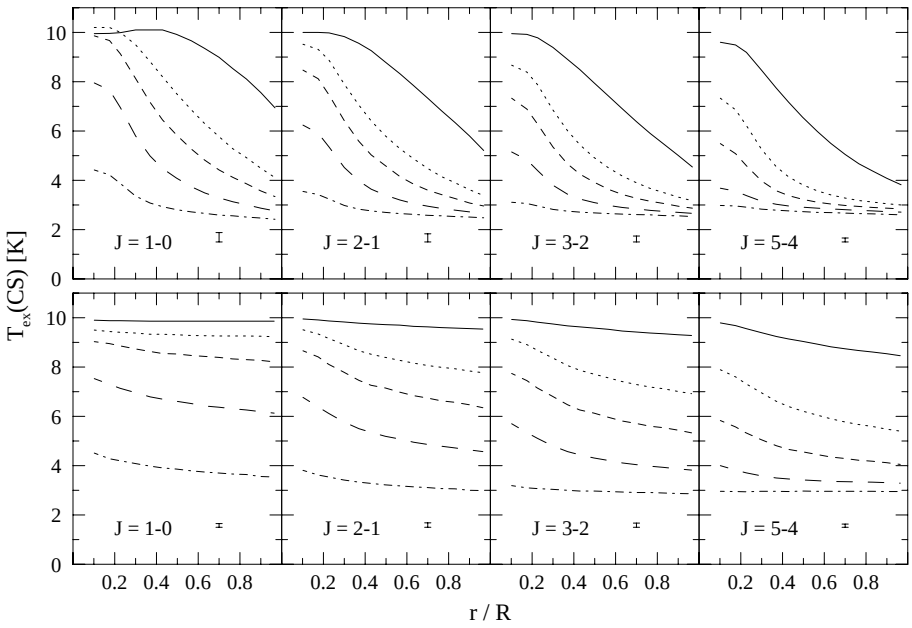

FIG. 1.—Radial variations of the CS excitation temperatures. The lower panel is for the CL models, while the upper panel is for the SM models. Solid, dotted, dashed, long-dashed, and dash-dotted lines, are for densities of $n^0_{H_2} = 3 \times 10^5$, 1×10^5, 6×10^4, 3×10^4, and $1 \times 10^4\ \mathrm{cm}^{-3}$, respectively. The error bars indicate $\pm 1\ \sigma$ levels of noises near $r/R = 0.5$.

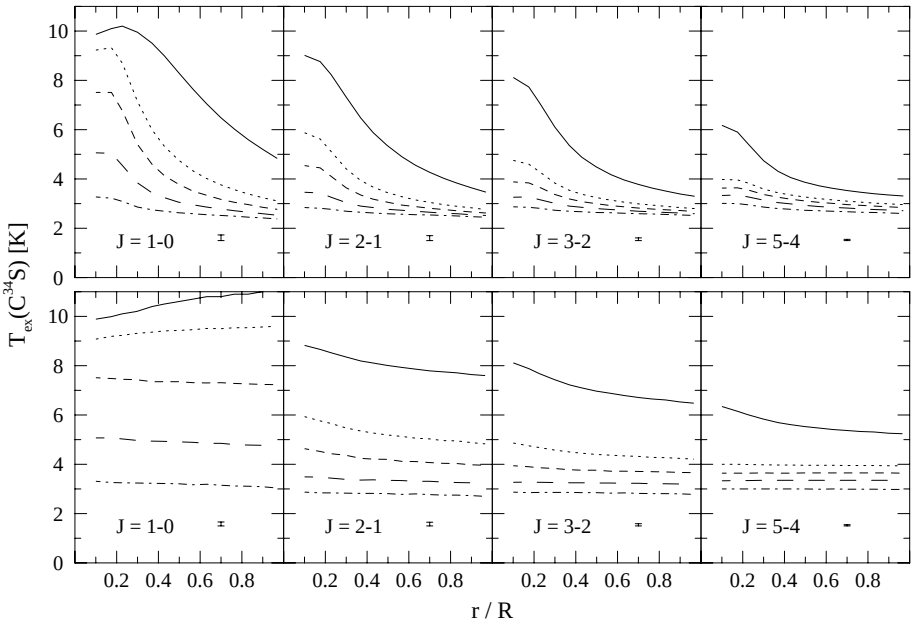

FIG. 2.—Same as Fig. 1, but for $C^{34}S$

take an average of 29 line profiles from a central disk whose radius is 3 units in cell size. In the case of the CL models, within this cylinder-like volume, there are ~ 330 clumps, and the mean volume filling factor is $\bar{f} \simeq 0.40$. Bulk velocity distributions of the clumps (CL model) and cells (SM model) in this volume are shown in the figure for reference.

The CS line profiles of the CL model exhibit flat-top features with bumps in the case of high density, $n^0_{H_2} \gtrsim 3 \times 10^5$ cm^{-3}. For the low-density model, the lines tend to mimic the bulk velocity distribution. As density increases, saturation takes place in the line center. However, the saturation does not lead to self-absorption for the CL model because T_{ex} stays nearly flat over the entire region. On the contrary, the SM model, which has a steep gradient of T_{ex}, shows self-absorption features, although optical depths are almost the same for both models (Table 1). Lines of the $J = 2$–1 and $J = 3$–2 transitions have deeper self-absorptions than those of the $J = 1$–0 and $J = 5$–4 transitions, because the former transitions are more opaque than the latter ones. The bumpy structure and asymmetries of line profiles common to both models are caused by the bulk motions of a finite number of clumps or cells. Optically thick lines are subject to local effects, since they are formed in the region of $\tau \sim 1$. The clumps or cells in the outskirts of the core make pedestals in the line wings, as can be inferred from the radial dependence of $\sigma_{blk}(r)$. Generally the lines of

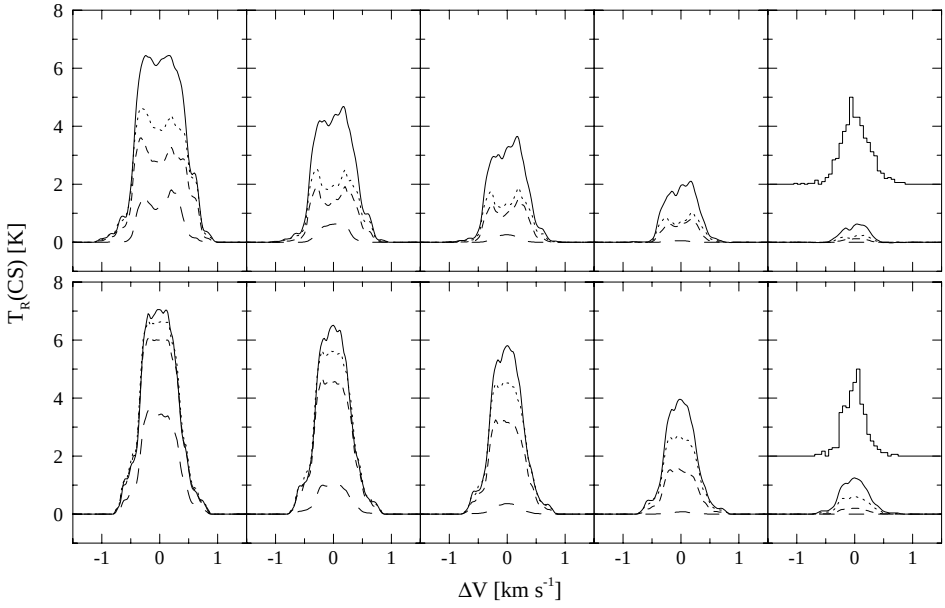

FIG. 3.—Line profiles of the CS from the center of the core. CL models are presented in the lower panel, SM models in the upper panel. Each frame represents, from left to right, those of $n^0_{H_2} = 3 \times 10^5$, 1×10^5, 6×10^4, 3×10^4, and 1×10^4 cm^{-3}, respectively. In the figure, solid, dotted, dashed, and long-dashed lines are for the $J = 1$–0, 2–1, 3–2, and 5–4 transitions, respectively. The line profiles are averaged over a central disk with 3 cell radius. In that disk a total of 29 rays are included. The bulk velocity distribution of clumps (CL model) or cells (SM model) in the cylindrical volume through which line emission is emanating is illustrated in the far right panels. The scale is arbitrary.

TABLE 1

LINE-CENTER OPTICAL DEPTHS OF SYNTHESIZED LINE PROFILES

		CL MODEL					SM MODEL				
MOLECULE	TRANSITION	30	10	6	3	1	30	10	6	3	1
CS	1–0	22.5	8.79	6.29	4.78	3.70	21.5	9.63	7.69	6.12	4.13
	2–1	63.6	25.1	18.3	13.2	7.13	62.5	28.5	21.4	14.6	6.86
	3–2	82.9	32.1	22.4	12.8	3.51	80.9	32.6	21.6	11.3	2.91
	5–4	36.2	10.1	3.53	0.55	0.03	31.1	6.90	2.24	0.32	0.02
$C^{34}S$	1–0	1.28	0.61	0.52	0.45	0.27	1.46	0.86	0.71	0.54	0.27
	2–1	4.24	2.41	1.82	1.12	0.40	4.68	2.54	1.82	1.05	0.37
	3–2	5.33	2.19	1.25	0.52	0.13	5.18	1.91	1.06	0.44	0.12
	5–4	1.09	0.09	0.03	0.01	0.00	0.78	0.06	0.02	0.01	0.00

NOTE.—Lines are averaged from profiles coming from the central disk whose radius is 3 cells long. Listed values are for densities of 30, 10, 6, 3, and 1 ($\times 10^4$ cm^{-3}).

the CL model, as well as the integrated intensities, are stronger than those of the SM model. Because of the self-absorption, the line becomes wider for the SM model than for the CL model.

Synthesized line profiles of the $C^{34}S$ transitions are shown in Figure 4, which are in contrast to the profiles of Figure 3 in the sense of having no flat top or self-absorption features. In optically thin transitions, emissions from each clump or cell are simply added together. Therefore, the resulting line profiles will resemble the distribution of bulk motion without showing wiggles. The line shapes, particularly of the CL models, are indeed similar to the bulk velocity distribution, as displayed in the figure. For the SM model we notice small humps in the $J = 2-1$ and $J = 3 - 2$ transitions with $n^0_{H_2} = 3 \times 10^5$ cm^{-3}. The humps result from a combination of high T_{ex} and large optical depth of a few cells corresponding to that velocity bin. The peak or integrated intensities of the CL model are generally greater than those of the SM model, while the line widths are similar to each other as shown in Table 2. It was found that the $C^{34}S$ $J = 5 - 4$ line, except for the highest density model, is generally weak to the level of a few tens of millikelvins. Therefore, the $C^{34}S$ transitions with J greater than 5 may be of little use in probing the dense cores.

Returning to the line profiles of CS, we compare the line widths and intensities among different transitions and between the two models. In the CL models, the ratios of $J = 3 - 2$ line width to $J = 2 - 1$ are roughly close to unity regardless of density, while in the SM models they are not (Table 2). In addition, the $J = 2 - 1$ lines are generally broader than the $J = 1 - 0$ lines for both models. These can be explained in terms of their optical depths. In the case of the SM model, except for the least dense model, the ratios of peak and integrated intensities of $J = 3 - 2$ to $J = 2 - 1$ lines are kept rather constant around 0.8 and 0.7, respectively. However, for the CL model, they vary widely with $n^0_{H_2}$. Observations show that the peak intensity ratio ranges between 0.3 and 0.5 (Zhou et al. 1989). For the $J = 2 - 1$ to $J = 1 - 0$ intensity ratio, it is between 0.5 (0.4) and 0.9 (0.7) for the CL (SM) model. In the observation, it varies from 0.2 to 0.6, but a large conversion factor (~ 10) from antenna to radiation temperature of the $J = 1 - 0$ transition makes these values uncertain (Fuller 1989). The peak intensity of $J = 2 - 1$ transition was observed to 2.3 K, significantly lower than the value of this work (Fuller 1989; Zhou et al. 1989). The volume filling factor of our model may be too large, particularly in the central part of the core. Since observation with a sharper beam tends to make the line

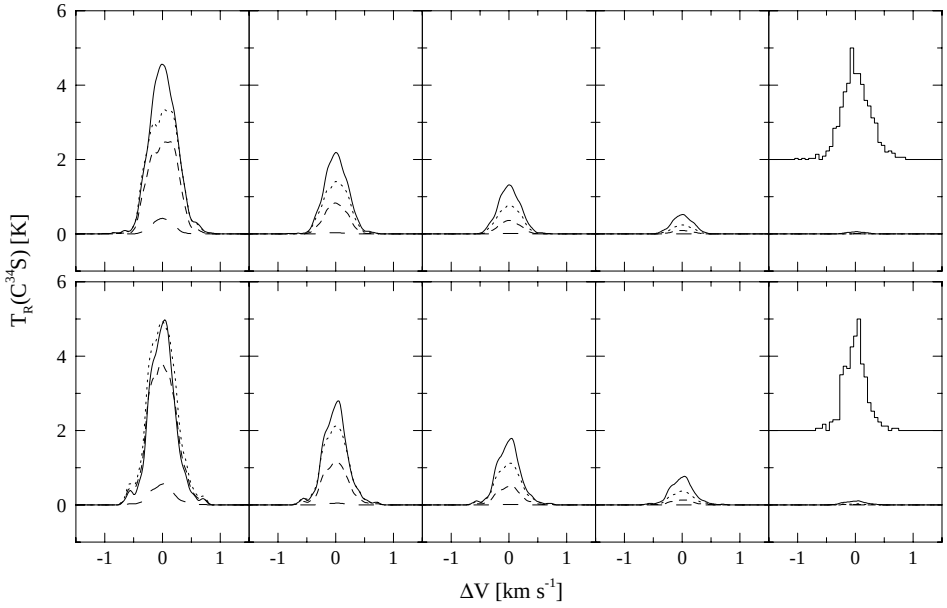

FIG. 4.—Same as Fig. 3, but for $C^{34}S$

TABLE 2

LINE PARAMETERS OF SYNTHETIC PROFILES

MOLECULE	TRANSITION	CL MODEL					SM MODEL				
		30	10	6	3	1	30	10	6	3	1
		Line Width (km s^{-1})									
CS	1–0	0.70	0.64	0.61	0.58	0.55	0.93	0.83	0.77	0.70	0.51
	2–1	0.72	0.70	0.68	0.64	0.59	1.01	0.91	0.86	0.76	0.57
	3–2	0.75	0.71	0.68	0.63	0.53	0.99	0.89	0.79	0.66	0.48
	5–4	0.71	0.61	0.52	0.42	...	0.81	0.58	0.46	...	...
$C^{34}S$	1–0	0.48	0.45	0.45	0.45	0.44	0.55	0.47	0.45	0.42	0.37
	2–1	0.58	0.53	0.51	0.47	...	0.68	0.53	0.49	0.43	...
	3–2	0.58	0.51	0.48	0.46	...	0.65	0.47	0.44	0.40	...
	5–4	0.46	...	...	...	...	0.42	...	...	...	...
		Peak Intensity (K)									
CS	1–0	7.05	6.51	5.81	3.96	1.25	6.44	4.68	3.65	2.10	0.63
	2–1	6.63	5.64	4.56	2.70	0.60	4.64	2.53	1.89	1.04	0.24
	3–2	6.01	4.69	3.25	1.57	0.20	3.60	1.92	1.47	0.79	0.12
	5–4	3.48	1.06	0.36	0.08	...	1.81	0.63	0.26	...	...
$C^{34}S$	1–0	4.98	2.80	1.79	0.77	0.11	4.56	2.19	1.32	0.52	0.06
	2–1	4.94	2.12	1.12	0.37	...	3.34	1.41	0.77	0.24	...
	3–2	3.80	1.15	0.51	0.13	...	2.47	0.83	0.36	0.09	...
	5–4	0.57	...	...	...	...	0.42	...	...	...	...
		Integrated Intensity (K km s^{-1})									
CS	1–0	5.51	4.59	3.89	2.53	0.73	6.44	3.82	2.66	1.38	0.31
	2–1	5.54	4.39	3.40	1.91	0.37	4.73	2.16	1.38	0.66	0.12
	3–2	5.09	3.61	2.39	1.06	0.11	3.44	1.52	1.00	0.48	0.06
	5–4	2.72	0.68	0.20	0.04	...	1.27	0.37	0.12	...	...
$C^{34}S$	1–0	2.60	1.34	0.84	0.36	0.05	2.66	1.09	0.62	0.23	0.02
	2–1	3.07	1.19	0.60	0.18	...	2.28	0.77	0.38	0.10	...
	3–2	2.40	0.62	0.26	0.06	...	1.62	0.41	0.16	0.04	...
	5–4	0.28	...	...	...	...	0.18	...	...	...	...

NOTE.—Line parameters whose peak intensities are less than 0.05 K are not tabulated. Listed values are for densities of 30, 10, 6, 3, and 1 ($\times 10^4$ cm^{-3}).

stronger, there may be a significant beam dilution (Mardones et al. 1997).

The self-absorption feature for the cold cores has been rarely observed. The comparison of line shapes and parameters seems to suggest that the CL model better describes the observations. However, recently the self-absorbed lines are being discovered frequently in the high spectral resolution survey of the cold cores with and without embedded stars in the CS $J = 2$–1 transition (Mardones et al. 1997; Lee et al. 1997). They are also found in other transitions such as HCO^+ and H_2CO (Gregersen et al. 1997; Mardones et al. 1997). Thus the internal structure of such cold cores may be similar to that of the SM model. Actually the self-absorption is a natural consequence of a smoothly varying system like the one-dimensional model of Liszt & Leung (1977). The point in question is how to explain line profiles without the self-absorption dip. Here we suggest that the line can exhibit a single peak feature even in the opaque transition if the system is clumpy and under macroturbulence.

4. DISCUSSION

4.1. *Comparison with LVG and LTE Analyses*

We may be able to locate line parameters of the synthesized profiles on the LVG grid in order to determine the hydrogen number density and abundance of the model cores. These can then be compared with values actually used in the model calculations. In this way one can assess the accuracy of the LVG analysis.

If we restrict comparisons to the case of more abundant species, CS, there are four transitions available. But the $J = 5 - 4$ line is generally too weak to be used as a probe of the core. We are thus left with three transitions. On the other hand, the LVG model is fully described by two parameters, i.e., the hydrogen number density, n_{H_2}, and the abundance divided by the velocity gradient, $X(\mathrm{CS})/(dV/dR)$. Here the kinetic temperature is assumed to be known a priori. Since, in an observational sense, taking the ratio of line parameters between different transitions involves a much smaller calibration error than merely using the radiation temperature itself, converted from the antenna temperature, it is sensible to make the LVG grids in terms of, e.g., $\int T_R(1\text{–}0)dv/\int T_R(2\text{–}1)dv$ and $\int T_R(3\text{–}2)dv/\int T_R(2\text{–}1)dv$. Figure 5 shows the contours of constant integrated intensity ratios, where filled circles represent the ones determined by the line parameters of five CL models. We adopt $\Delta V \simeq 0.8$ km s^{-1} from Figure 3 and $\Delta R \simeq 0.2$ pc, and the diagram gives the abundance in the range of 4×10^{-10} to 4×10^{-9}, which is an underestimate by a factor of up to 10. On the other hand, derived hydrogen number density is close to the clump density.

It should be pointed out that there is no cross point between two types of contours for the line parameters of the SM models. When uncertainty such as observational noise is included, the solid and dotted lines may meet each other in the lower right part of the diagram. However, in this case, core properties cannot be uniquely determined, since two types of contours run almost parallel to each other. These findings seem to be natural; in the CL model internal condi-

tion is relatively uniform, and the clumps are radiatively decoupled from each other due to their large bulk motions. Therefore, the CL model is somewhat compatible with the assumption of the LVG model, while the SM model is not. Thus, the success or failure of the LVG fitting in several sources may be understood in terms of their internal structure (Snell et al. 1984; Zhou et al. 1989; Zhou et al. 1994b; Zhou et al. 1991; Wang et al. 1993; Plume et al. 1997).

When only one transition is observed for both CS and $C^{34}S$, the LTE approximation is often employed for the estimation of column density. Assuming the abundance ratio of 20 and the same excitation temperature for both species, one can find the optical depth of $C^{34}S$ and the excitation temperature for the transition. We carried out the same type of LTE analysis with the line parameters of synthesized profiles and summarized results in Table 3. When compared with those in Table 1, the optical depth is roughly consistent only for the $J = 1 - 0$ transitions of both kinds of models, and they differ by a factor up to ~ 5 in higher transitions. From Figure 2 and Table 3, we notice that the derived LTE excitation temperature is generally higher for all transitions of the CL models and for higher transitions of the SM models. Thus we may expect that LTE analysis yields reasonable estimates of the $C^{34}S$ column density only for lower transitions. The derived column densities are shown in Table 3 and compared with those calculated from model parameters. For the $J = 1$–0 transition, the LTE column density differs from the true value by a few times 10%, which is similar to what we have seen in the case of CO (Park & Hong 1995; Park et al. 1996). On the other hand, the values derived by higher transitions differ by a factor of 10, at most. It results mainly from the invalid assumption of the same excitation temperature for CS and $C^{34}S$.

4.2. *Inferring Information of Clumps*

Tauber (1996) has developed a method for deriving such clump parameters as the optical depth, excitation temperature, and size of the clump, including the total number of clumps in a telescope beam. We will apply his method to our synthesized profiles for the four CL models and examine how accurately his method recovers the clump parameters employed in model calculations. His assumption on a model cloud or core is very similar to ours. The model cloud is composed of many small clumps that may have internal density structure. The clumps have internal as well as bulk motions, as we assumed. For this model, he showed how these clump parameters are related to the line intensity, the line width, and the smoothness ratios between optically thin and thick transitions, where the smoothness is defined as the standard deviation of a fluctuating line profile with respect to a certain smoothed line profile. Three ratios are derived from basic equations (Tauber 1996),

$$T_R \simeq T_{\rm ex}(1 - e^{-\tau_{\rm ef}}) , \tag{3}$$

where

$$\tau_{\rm ef} = N r_0^2 (\sigma_{\rm thr}/\sigma_{\rm blk}) A(\tau_0) \exp\left[- (v/\sigma_{\rm blk})^2 \right] . \tag{4}$$

Here τ_0 is the line-center optical depth of rarer isotope through the center of a clump, N is the number of clumps per unit area along a line of sight, and r_0 is the radius of a spherical clump. $A(\tau_0)$ depends on the internal density structure of a clump and is found in Martin et al. (1984).

Actually Martin focuses on the smoothness of the line profile, since it is most sensitive to the clump parameters. However, the smoothness is found to be of no use in our case because fixing an average profile is too subjective. Thus we concentrate mainly on the ratios of line width and intensity. Adopting a hard sphere model, close to our CL model of uniform density, we plot the contours of constant peak intensity and line width ratios in Figure 6, corresponding to Tauber's Figure 2, differing in the abundance ratio.

Using the pairs of CS and $C^{34}S$ transitions in Table 2, we could find the values of $N_v = N r_0^2 (\sigma_{\rm thr}/\sigma_{\rm blk})$ and τ_0 as shown in Table 4. Here we use the $J = 1 - 0$ and $J = 2 - 1$ transition only. Then r_0 can be found, since τ_0 is related to it (Tauber 1996). A partition function and $T_{\rm ex}$ needed in this process are obtained by the LVG approximation. The r_0 is converted to $l = (4\pi/3)^{1/3} r_0$, the size of a cube whose volume is the same as a sphere with radius r_0. It is compared to the size of the cubic cell of our models, $l' = (0.6/31)$ pc = 0.019 pc in Table 4. On the other hand, the total number of clumps in a telescope beam is calculated from the relation $N_{\rm tot} = N_v (\sigma_{\rm blk}/\sigma_{\rm thr})$(beam area$/r_0^2$), where $\sigma_{\rm thr} = 0.062$ km s^{-1} and $\sigma_{\rm blk}$ is approximated as 0.4 km s^{-1} from Table 2. Consequently the volume filling factor of clumps in

TABLE 3

LINE CENTER OPTICAL DEPTH, EXCITATION TEMPERATURE, AND COLUMN DENSITY

	CL MODEL				SM MODEL			
PARAMETER	30	10	6	3	30	10	6	3
τ (1–0)	1.22	0.56	0.37	0.21	1.24	0.63	0.45	0.28
τ (2–1)	1.37	0.47	0.28	0.14	1.27	0.82	0.52	0.26
τ (3–2)	1.00	0.28	0.16	0.06	1.16	0.57	0.28	0.11
$T_{\rm ex}$ (1–0) (K)	9.88	9.35	8.60	6.86	9.23	7.49	6.44	4.90
$T_{\rm ex}$ (2–1) (K)	9.77	8.78	7.69	5.86	7.75	5.53	4.87	3.94
$T_{\rm ex}$ (3–2) (K)	9.64	8.28	6.92	5.62	7.09	5.21	4.69	3.94
$N_{\rm LTE}$ (1–0)[a] / 10^{13} (cm^{-2})	4.47	1.88	1.08	0.41	4.52	1.45	0.76	0.27
$N_{\rm LTE}$ (2–1)[a] / 10^{13} (cm^{-2})	2.08	0.62	0.30	0.10	1.55	0.54	0.28	0.10
$N_{\rm LTE}$ (3–2)[a] / 10^{13} (cm^{-2})	1.27	0.29	0.14	0.05	1.21	0.42	0.20	0.08
$N_{\rm true}$ / 10^{13} (cm^{-2})	4.10	1.37	0.82	0.41	4.10	1.37	0.82	0.41

NOTE.—Derived for the $C^{34}S$ by applying the LTE method to the synthesized line profiles. Listed values are for densities of 30, 10, 6, and 3 ($\times 10^4$ cm^{-3}).

[a] $N_{\rm LTE}$ (i–j) is the *total* column density of the $C^{34}S$ obtained from the transition i to j.

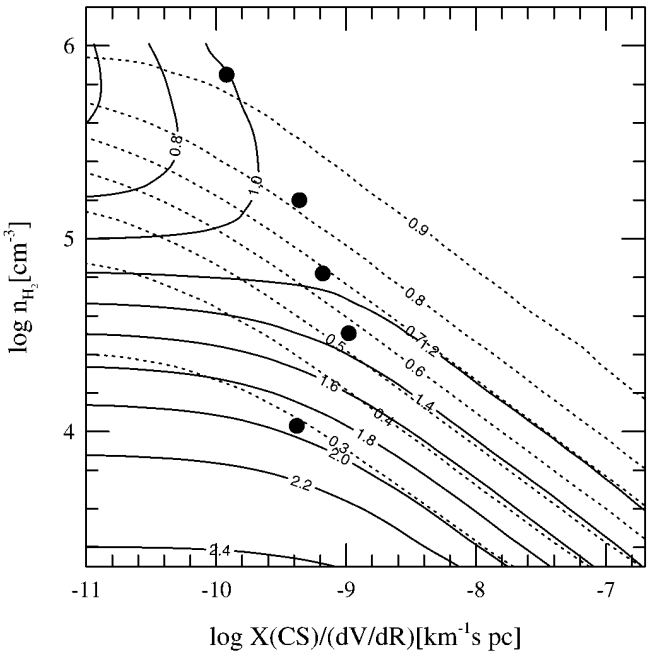

FIG. 5.—Results of the LVG run with T_k of 10 K. The solid lines are the contours of constant $\int T_R(1\text{–}0)dv/\int T_R(2\text{–}1)dv$, and the dotted lines, $\int T_R(3\text{–}2)dv/\int T_R(2\text{–}1)dv$. Filled circles are determined by the line parameters of five CL models; from top to bottom, $n^0_{H_2} = 3 \times 10^5$, 1×10^5, 6×10^4, 3×10^4, and 1×10^4 cm^{-3}, respectively. We could not find such cross points for the SM models.

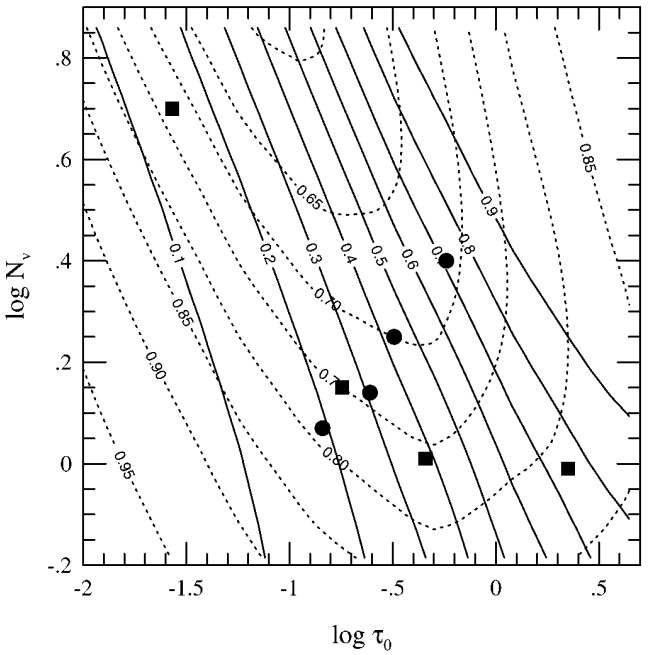

FIG. 6.—Contours of constant peak intensity (*solid lines*) and line width ratios (*dotted lines*) for the CS and C^{34}S pairs are shown as functions of N_v and τ_0. (see text for details). Dots represent four cases of the CL model for $J = 1\text{–}0$ transitions. From right to left, $n^0_{H_2} = 3 \times 10^5$, 1×10^5, 6×10^4, and 3×10^4 cm^{-3}, respectively. Squares are for $J = 2\text{–}1$ transitions, and the designation of $n^0_{H_2}$ is in the opposite order.

the beam is given by $f \simeq [N_{tot}/(29 \times 31)] \times (l/l')^3$. These values are summarized in Table 4. It was shown that much of the original information on the clump characteristics could be recovered within a factor of 2–3, although we started from very rough assumptions. Erroneous estimates are also noted, and the main cause of discrepancy can be found in Figures 1 and 2, where the assumption of uniformity and coincidence between two transitions of T_{ex} is no longer valid.

4.3. *Interpreting Infall Signature*

The SM model deserves attention in the context of spectroscopic signature of infall motion. To claim an infall motion as evidence of collapsing dense cores, one has to show at least the following observational facts: (1) self-absorption of an opaque line with a stronger blue peak, (2) a single peak of optically thin line located between the two peaks of the opaque line, and (3) the larger width of lines tracing higher density. Moreover, these features should be conspicuous toward the center. However, usually a combination of (1) and (2) are mentioned in the previous studies. But our calculation (Figs. 3 and 4) shows that (1) and (2) can be obtained without infall motion. (The depth of self-absorption and the degree of asymmetry can be even stronger with steeper gradients of T_k and density.) Thus the observational features considered as evidence of inward motion should be accepted with some caution. In this respect, it should be noted that double peaks with a stronger red peak are often observed, and that a stronger peak often switches from blue to red and vice versa in the maps of many sources, including B335 and L1527 (Kameya et al. 1985; Mardones et al. 1994; Myers et al. 1995; Lee et al. 1997). Moreover, there are sources where an asymmetry changes from transition to transition (Mardones et al. 1997; Gregersen et al. 1997; Lehtinen 1997). In fact, many asym-

TABLE 4

CLUMP PARAMETERS[a]

	$J = 1 - 0$				$J = 2 - 1$				
PARAMETER	30	10	6	3	30	10	6	3	Model Value
τ_0(C^{34}S).....	0.58	0.32	0.25	0.14	2.2	0.46	0.18	0.027	...
N_v	2.5	1.8	1.4	1.2	0.98	1.0	1.4	5.0	...
l(pc)	0.069	0.040	0.032	0.014	0.074	0.013	0.0061	0.0011	0.019
N_{tot}	95	200	250	1000	32	1100	6900	730000	330
f	5.1	2.1	1.3	0.49	2.1	0.38	0.25	0.16	0.40

NOTE.—$J = 1\text{–}0$ and $J = 2\text{–}1$ lines are used independently to derive these parameters. Listed values are for densities of 30, 10, 6, and 3 ($\times 10^4$ cm^{-3}).

[a] Obtained by applying the method of Tauber 1996.

metric profiles are not fitted well with (microturbulent) models under the assumption of spherical symmetry (Myers et al. 1995). The asymmetry may take place simply because an optically thick line is sensitive to the local property. These facts suggest that departure from the (implicitly assumed) spherical symmetry, both in density and in the distribution of micro- and macro-motion, should be taken into account in analyzing the infall candidates.

5. SUMMARY AND CONCLUSION

We have constructed two heuristic dense core models: the CL model for clumpy structured cores and the SM model for completely filled cores. By applying the three-dimensional non-LTE radiative transfer code, we examined the excitation status and resulting emission lines of the CS rotational transitions.

The excitation conditions of CS are found to be rather uniform in the CL model, while the excitation temperature drops rapidly outward in the SM model. The resulting line profiles of CS have a wiggly flat top in the CL model, but a self-absorption dip in the SM model. But for both models, the $C^{34}S$ lines exhibit a single peak resembling the bulk velocity distribution of the clumps or cells.

An application of the LVG model to synthesized lines is found to guarantee a reasonable estimate of the abundance and density of the cores for the CL model, whereas it is not so for the SM model. We note that the method by Tauber (1996) is good enough to make rough estimates on the clump size, the filling factor, and the number of clumps in a certain volume.

It is interesting to note that the detection rate of self-absorption of a CS line is less than 10% in the warm dense cores in the region of massive star formation where steep density and temperature gradient are likely to appear (Juvela 1996; Zinchenko et al. 1994; Zinchenko et al. 1995). On the other hand, in the survey of starless dense cores by Lee et al. (1997), more than 50% of the sources exhibit self-absorption features. A survey of low-mass star-forming cores suggests that the rate is much higher in class 0 sources than in class I sources (Mardones et al. 1997). A large amount of turbulence caused by, e.g., outflows and winds may get rid of an absorption dip in the warm cores. The difference between the class 0 and class I sources may be related to their evolutionary stage (Mardones et al. 1997). The CL and SM models or their combination may provide a clue in understanding the internal structure and/or dynamical evolution of the cores.

S.-S. H. was supported by the Korean Ministry of Education through Research Fund BSRI-96-5411, and Y. S. P. was supported by Korea Astronomy Observatory (96-5400-000).

REFERENCES

Caselli, P., & Myers, P. C. 1995, ApJ, 446, 665
Fuller, G. A. 1989, Ph.D. thesis, Univ. California, Berkeley
Fuller, G. A., & Myers, P. C. 1992, ApJ, 384, 523
Goodman, A. A., Benson, P. J., Fuller, G. A., & Myers, P. C. 1993, ApJ, 406, 528
Green, S., & Chapman, S. 1978, ApJS, 37, 169
Gregersen, E. M., Evans, N. J., II, Zhou, S., & Choi, M. 1997, ApJ, 484, 256
Juvela, M. 1996, A&AS, 118, 191
———. 1997, A&A, 322, 943
Kameya, O., Hasegawa, O., Hirano, N., Takakubo, K., & Seki, M. 1985, in IAU Symp. 115, Star-forming Regions, ed. M. Peimbert & J. Jugaku (Dordrecht: Reidel), 366
Kwan, J., & Sanders, D. B. 1986, ApJ, 309, 783
Lee, C. W., et al. 1997, in preparation
Lehtinen, K. 1997, A&A, 317, L5
Liszt, H. S., & Leung, C. M. 1977, ApJ, 218, 396
Mardones, D., Myers, P. C., Caselli, P., & Fuller, G. A. 1994, in Clouds, Cores, and Low Mass Stars, ed. D. P. Clemens & R. Barvainis (San Francisco: ASP), 192
Mardones, D., Myers, P. C., Tafalla, M., Wilner, D. J., Bachiller, R., & Garay, G. 1997, ApJ, 489, 719
Martin, H. M., Sanders, D. B., & Hills, R. E. 1984, MNRAS, 208, 35
Myers, P. C., Bachiller, R., Caselli, P., Fuller, G. A., Mardones, D., Tafalla, M., & Wilner, D. J. 1995, ApJ, 449, L65
Myers, P. C., & Benson, P. J. 1983, ApJ, 266, 309
Myers, P. C., Linke, R. A., & Benson, P. J. 1983, ApJ, 264, 517
Park, Y.-S., & Hong, S. S. 1995, A&A, 300, 890
Park, Y.-S., Hong, S. S., & Minh, Y. C. 1996, A&A, 312, 981
Plume, R., Jaffe, D. T., Evan, N. J., II, Martín-Pintado, J., & Gómez-González, J. 1997, ApJ, 476, 730
Shu, F. H. 1977, ApJ, 214, 488
———. 1991, in The Physics of Star Formation and Early Stellar Evolution, ed. C. J. Lada & N. D. Kylafis (Dordrecht: Kluwer), 365
Shu, F. H., Adams, F. C., & Lizano, S. 1987, ARA&A, 25, 31
Snell, R. D., Mundy, L. G., Goldsmith, P. F., Evans, N. J., II, & Erickson, N. R. 1984, ApJ, 276, 625
Tauber, J. A. 1996, A&A, 315, 591
Walker, C. K., Narayanan, G., & Boss, A. P. 1994, ApJ, 431, 767
Wang, Y., Jaffe, D. T., Evans, N. J., II, Hayashi, M., Tatematsu, K., & Zhou, S. 1993, ApJ, 419, 707
Zhou, S. 1995, ApJ, 442, 685
Zhou, S., Butner, H. M., Evans, N. J., II, Güsten, R., Kutner, M. L., & Mundy, L. G. 1994b, ApJ, 428, 219
Zhou, S., Evans, N. J., II, Kömpe, C., & Walmsley, C. M. 1993, ApJ, 404, 232
———. 1994a, ApJ, 421, 854
Zhou, S., Evans, N. J., II, & Wang, Y. 1996, ApJ, 466, 296
Zhou, S., Evans, N. J., II, Güsten, R., Mundy, L. G., & Kutner, M. L. 1991, ApJ, 372, 518
Zhou, S., Wu, Y., Evans, N. J., II, Fuller, G. A., & Myers, P. C. 1989, ApJ, 346, 168
Zinchenko, I., Forsström, V., Lapinov, A., & Mattila, K. 1994, A&A, 288, 601
Zinchenko, I., Mattila, K., & Toriseva, M. 1995, A&AS, 111, 95